Electric Propulsion System Optimization for Long-Endurance and Solar-Powered Unmanned Aircraft

Or D. Dantsker[*] and Marco Caccamo [†]

Technical University of Munich, Garching, Germany

Saym Imtiaz[‡]

University of Illinois at Urbana–Champaign, Urbana, IL 61801

The increase in popularity of unmanned aerial vehicles (UAVs) has been driven by their use in civilian, education, government, and military applications. However, limited on-board energy storage significantly limits flight time and ultimately usability. The propulsion system plays a critical part in the overall energy consumption of the UAV; therefore, it is necessary to determine the most optimal combination of possible propulsion system components for a given mission profile, i.e. propellers, motors, and electronic speed controllers (ESC). Hundreds of options are available for each of the components with generally non-scientific advice for choosing the proper combinations. This paper describes a propulsion system optimization tool that determines the optimal propeller and motor combination(s) for an electric, fixed-wing unmanned aircraft, given desired mission requirements. Specifically, missions are broken down into expected segments with velocity and thrust requirements being computed using a high-fidelity aircraft power model. The optimization tool then estimates the required propeller rotation rate, followed by the power consumption for each segment and propeller-motor combination. It then integrates the segment results into missions for each combination and tabulates the results, sorting by overall efficiency. Among a variety of additional functionality integrated into the tool, the optimizer considers aircraft safety by estimating the maximum thrust each combination can produce, which is crucial in upset recovery scenarios such as stall. Experimental validation testing of the optimization tool was performed through flight testing of an aircraft. Additionally, propulsion system optimization of two simulated missions were performed, demonstrating significant energy saving that can be made; this is especially paramount for long-endurance, solar-powered aircraft.

Nomenclature

ESC	=	electronic speed controller	P_{shaft}	= shaft power
RPM	=	rotations per minute	P_{motor}	= thrust power
UAV	=	unmanned aerial vehicle	Q	= torque
			R	= universal gas constant
C_P	=	power coefficient	R_m	= internal motor resistance
C_T	=	thrust coefficient	T	= thrust
D	=	propeller diameter	t	= ambient temperature
i_m	=	motor current	V	= air flow velocity
i_0	=	zero load motor current	U_emf	= motor back emf voltage
J	=	advance ratio	U_m	= motor terminal voltage
K_v	=	motor speed constant		
n	=	propeller and motor rotation rate	η_{prop}	= propeller efficiency
p	=	ambient pressure	η_{motor}	= motor efficiency
P_{input}	=	input power	ρ	= density of air
P_{motor}	=	motor power		

---

[*]Researcher, Department of Mechanical Engineering, AIAA Student Member.
[†]Professor, Department of Mechanical Engineering.
[‡]Undergraduate Student, Department of Aerospace Engineering.

American Institute of Aeronautics and Astronautics

I. Introduction

In recent years, there has been an uptrend in the popularity of UAVs driven by the desire to apply these aircraft to areas such as precision farming, infrastructure and environment monitoring, surveillance, surveying and mapping, search and rescue missions, weather forecasting, and more. A key commonality across the aforementioned applications is the necessity of sensing. Notably, the majority of the aforementioned applications require continuous collection and processing of visual data (e.g. visible, IR, UV, and multi-spectral) . The traditional approach for small size UAVs is to capture data on the aircraft, stream it to the ground through a high power data-link, process it remotely (potentially off-line), perform analysis, and then relay commands back to the aircraft as needed.[1–3] Since the inception of unmanned aircraft, a key design constraint has been energy storage as limited on-board energy storage significantly limits flight time and ultimately usability. Given the finite energy resources found onboard an aircraft (battery or fuel), traditional designs greatly limit aircraft endurance as significant power is required for propulsion, actuation, and the continuous transmission of visual data.

To truly enable a variety of applications, the overarching goal is to create a computationally-intensive, long-endurance solar-powered unmanned aircraft that would carry a high-performance embedded computer system to perform all required computations online and only downlink final results, saving a significant amount of energy. Currently, such an aircraft is in development: UIUC Solar Flyer,[4,5] which is shown in Fig. 1. The completed 4.0 m (157 in) wingspan aircraft will weight approximately 2.5 kg (88 oz) and be instrumented with an integrated autopilot and high-fidelity data acquisition system with an integrated 3D graphics processing unit. Given the objective, to operate continuously during all-daylight hours, the aircraft will be powered by solar array, specifically gallium arsenide (GaAs) solar cells from Alta Devices, which hold the world record for solar efficiency and power density, will be used in conjunction with a maximum power point tracking (MPPT) charge controller and a small lithium polymer battery that will act as an energy buffer.
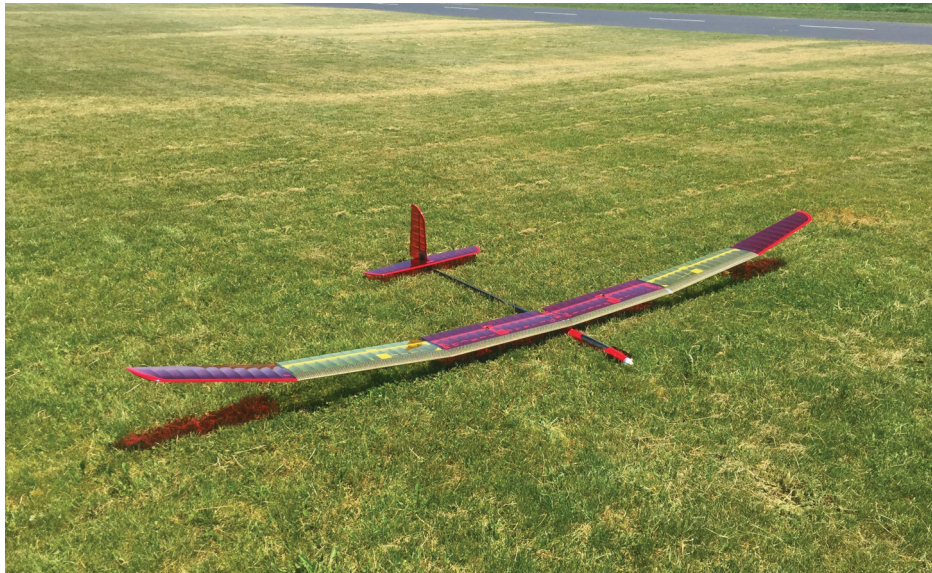
Figure 1: The baseline UIUC Solar Flyer aircraft shown without solar arrays.

American Institute of Aeronautics and Astronautics

The critical choice in the UIUC Solar Flyer's development then becomes what type of propulsion system to use. Therefore, it is necessary to determine the most optimal combination of possible propulsion system components for a given mission profile, i.e. propellers, motors, and electronic speed controllers (ESC). Hundreds of options are available for each of the components with generally non-scientific advice for choosing the proper combinations. To date, there has been significant effort in the modelling[6–8] and testing[9–23] of UAV propulsion system components. However, there has been comparatively limited effort put into optimizing the matching of these components,[24] mostly towards custom-designed or generic-shaped propellers.[25–28]

This paper describes a propulsion system optimization tool that determines the optimal propeller and motor combination(s) for an electric, fixed-wing unmanned aircraft, given desired mission requirements. Specifically, the process begins with a desired mission profile that is made up of segments with expected length, velocity, and climb and bank angle values. A high-fidelity power model is then used to translate the segment properties into sets of lengths, velocities, and thrust values. These final properties and the expected air density are input into the propulsion system optimization tool.

The tool is populated with databases of potential motors and propellers that may be used on the given unmanned aircraft. These databases contain information about each component, specifically motor parameters and propeller performance curves, which can be obtained from a variety of sources.The optimization tool then estimates the required rotation rate followed by the power consumption for each segment and propeller-motor combination. It then integrates the segment results into missions for each combination and tabulates the results, sorting by overall efficiency.

Among a variety of additional functionality integrated into the tool, the optimizer considers aircraft safety by estimating the maximum thrust that each combination can produce, which is crucial in upset recovery scenarios such as stall. Additionally, the tool is able to compute a combination's performance for a set or sweep of velocities and thrusts, either as required by a flight condition or from flight test data; this is helpful for mission planning and post-flight analysis. The optimization tool and its additional functionalities were experimentally validated through flight testing of a previously developed and well-characterized unmanned aircraft. Additionally, propulsion system optimization of two simulated missions was performed, demonstrating the energy saving that can be made.

This paper will first examine modeling methods for propellers and motors. Then the functionality of the propulsion system optimization tool will be discussed. This will be followed by flight testing validation of the tool. Next, propulsion system optimization for two simulated missions will be presented and discussed. Finally, a summary and statement of future work will be given.

American Institute of Aeronautics and Astronautics

II. Modeling

The propulsion system efficiency is equal to the product of the component efficiencies. In this paper, only the motor and propeller are considered. The relationship is summarized as follows:

$$P_{thrust} = \eta_{prop} \cdot \eta_{motor} \cdot P_{input} \tag{1}$$

Individual efficiencies are now examined including how they are derived from data. These efficiencies depend on numerous factors that are directly or indirectly related to the components, the aircraft flight state, and the environment.

It should be noted that a variety of methods exist[6, 20, 22] to calculate ESC efficiency. These generally yield that ESC efficiency is a function of voltage and current. Duty cycle, which is proportional to shaft rotation rate and/or throttle input, is often also taken into account. This and power supply efficiency (e.g. battery, solar cell, MPPT charge controller, etc.) are outside of the scope of the current work and could be incorporated at a later time.

A. Propeller

From the thrust, torque, rotation rate, and flow velocity values, the thrust coefficient, power coefficient, and propeller efficiency values are calculated. In order to perform these calculations, knowledge of the air density and propeller diameter is required. Using the temperature and pressure readings, the air density is determined using the equation of state

$$p = \rho R t \tag{2}$$

where R is the universal gas constant with a value for air of 287.0 $\mathrm{m^2/s^2/K}$ (1716 $\mathrm{ft^2/s^2/R}$).

The propeller advance ratio J is defined from the ratio of the measured air flow speed V to the propeller rotation rate n (in rev/s) and the propeller diameter D as

$$J = \frac{V}{nD} \tag{3}$$

The thrust coefficient C_T is calculated from the measured thrust T, rotation rate, air density, and the propeller diameter as

$$C_T = \frac{T}{\rho n^2 D^4} \tag{4}$$

In order to determine the power coefficient, propeller shaft output power P_{shaft} must be found. Propeller shaft power is determined from the measured torque Q and rotation rate by

$$P_{shaft} = 2\pi n Q \tag{5}$$

Therefore, the power coefficient C_P can be calculated from the measured rotation rate, propeller shaft power, air density, and propeller diameter as

$$C_P = \frac{P_{shaft}}{\rho n^3 D^5} \tag{6}$$

Finally, the propeller efficiency η_p can be determined as

$$\eta_{prop} = J \frac{C_T}{C_P} \qquad (7)$$

B. Motor

The motor efficiency is defined as the ratio between the shaft output power P_{shaft} and the motor input power P_{motor}.

$$\eta_{motor} = \frac{P_{shaft}}{P_{motor}} \qquad (8)$$

The shaft output power P_{shaft} can be computed using Equation 5, however, the torque and rotation rate must be known. The rotation rate is either set or measured. Equations 5 and 6 are combine to determine the torque

$$Q = \frac{C_P \rho n^2 D^5}{2\pi} \qquad (9)$$

Thus, it is assumed that the propeller rotation rate is set/measured and that the air density, propeller diameter, and propeller power coefficient are known. It should be noted that the power coefficient can be determined from performance curves with knowledge of current rotation rate and advance ratio (based on current velocity), both assumably set/measured.

Meanwhile, the motor input power P_{motor} is computed as the product of the motor voltage U_m and motor current i_m.

$$P_{motor} = U_m i_m \qquad (10)$$

From modeling of brushed DC motors, which has been applied to brushless DC motors,[8] the voltage is found as

$$U_m = U_{emf} + i_m R_m \qquad (11)$$

where U_{emf} is the back emf voltage and R_m is the motor internal resistance in Ohms. The back emf voltage is found by

$$U_{emf} = \frac{60n}{K_v} \qquad (12)$$

where K_v is the motor speed constant in RPM (rev/min) per Volt.

The current is calculated from the torque from Equation 9 and two motor parameters

$$i_m = i_0 + \frac{2\pi K_v Q}{60} \qquad (13)$$

where i_0 is the the motor current at zero load in Amperes.

Alternately, other methods exist to determine motor efficiency. For example, a first order approximation by Drela[29] estimates motor efficiency as a function of motor voltage and rotation rate, and the 3 aforementioned motor parameters.

$$\eta_{motor}(\Omega, U_m) = \left(1 - \frac{i_0 R_m}{U_m - 60n/K_v} \right) \frac{60n}{U_m K_v} \qquad (14)$$

A second order approximation[30] also exists, however, it requires a fourth motor parameter, K_Q, the motor torque constant, which is not easily obtained from manufacturers but instead needs to be measured through dynamometer benchtop testing.[22]

III. Functionality

The propulsion system optimization tool was primarily developed to match propeller and motor combinations to the requirements of a mission. However, the optimization tool also calculates the maximum thrust that each propeller motor combination can produce for a given minimum aircraft speed; this value is a key factor in evaluating whether a combination provides a desired level of safety for upset scenarios. Additionally, the tool is able to compute a combination's performance for a set or sweep of velocities and thrusts, either as required by a flight condition or from flight test data; this is helpful for mission planning and post-flight analysis. Below, each of the propulsion system optimization tool functionality are described in detail.

A. Mission Based Propulsion System Optimization

Missions are broken down into expected segments with velocity and thrust requirements. These velocity and thrust requirements are calculated using a previously developed high fidelity aircraft power model,[31] which requires three scalar variables, determined either from aircraft specifications or learned from a flight data set using linear regression. The desired mission flight states (velocities and thrusts), potential propeller data curves, and potential motor specifications are then fed into a propeller-motor efficiency algorithm. The entire *Mission Based Propulsion System Optimization* process and the *Flight Segment Propeller-Motor Efficiency Algorithm* can be visualized in Figs. 2 and 3, respectively.

For each mission segment, the *Flight Segment Propeller-Motor Efficiency Algorithm* determines the rotation rate required for each propeller to achieve the desired thrust at the given velocity using the *Propeller Rotation Rate Subroutine*. It does so by iteratively running along the thrust coefficient curves on the propeller performance plots, finding points that produce the closest thrust coefficient values required to achieve the desired thrust, and then interpolating between curves. These propeller performance curves are created using databases of possible propellers, which can be accumulated from a variety of sources including experimentally-validated analytical methods,[32] BEMT results,[25,33] and wind tunnel data.[34,35] A diagram of the *Propeller Rotation Rate Subroutine* is shown in Fig. 4 and example propeller performance curves are shown in Fig. 5.

Once the rotation rate is found for each propeller, the value is used to determine the shaft-to-thrust conversion efficiency of each propeller; this is done by interpolating the power coefficient for each propeller from their respective curves, and then using Equation 7. A specification-based analytical motor model, developed from the theory presented in Section II.B, is then used to calculate the electric power-to-shaft power conversion efficiencies for each of the possible motors. This process occurs for each of the motors, with each of the possible propeller, at each of their respective rotation rates, for all of the segments.

Finally, a table of possible motor and propeller combinations is generated. This table includes the total energy required as well as the total-averaged conversion efficiency for each propeller motor combination. Since flight missions contain multiple segments, each having different thrust and velocity requirements, the energy requirement for each segment is computed independently and then summed together. This value is then divided by the total output energy that propelled the aircraft yield the total-averaged efficiency for the total mission. The best combinations can be chosen for each mission.
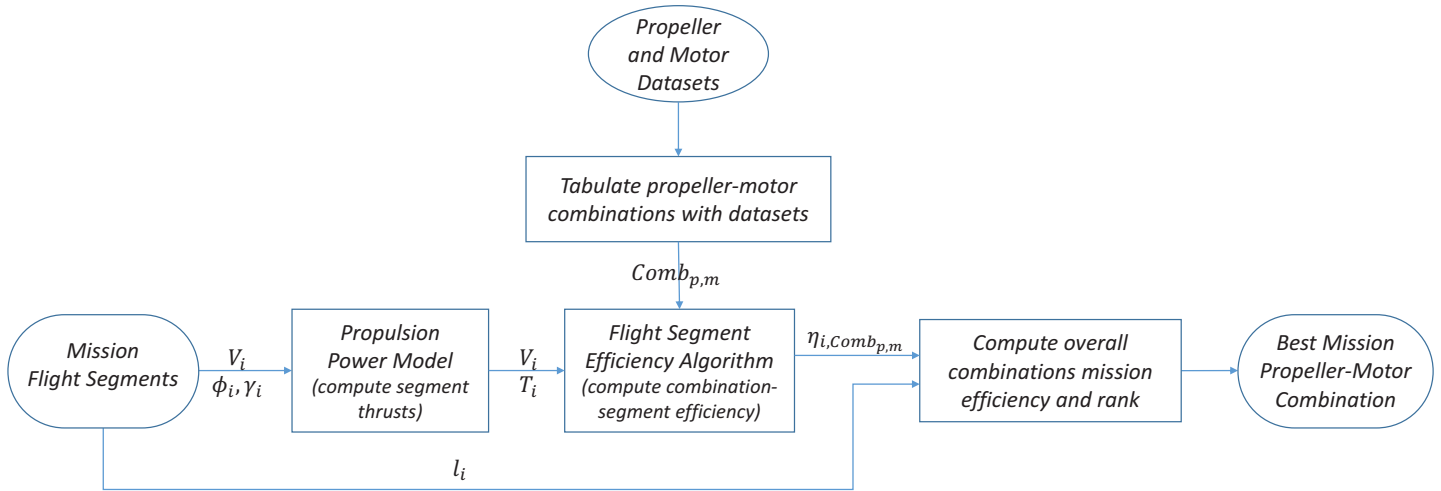
Figure 2: Process diagram for the *Mission Based Propulsion System Optimization*.
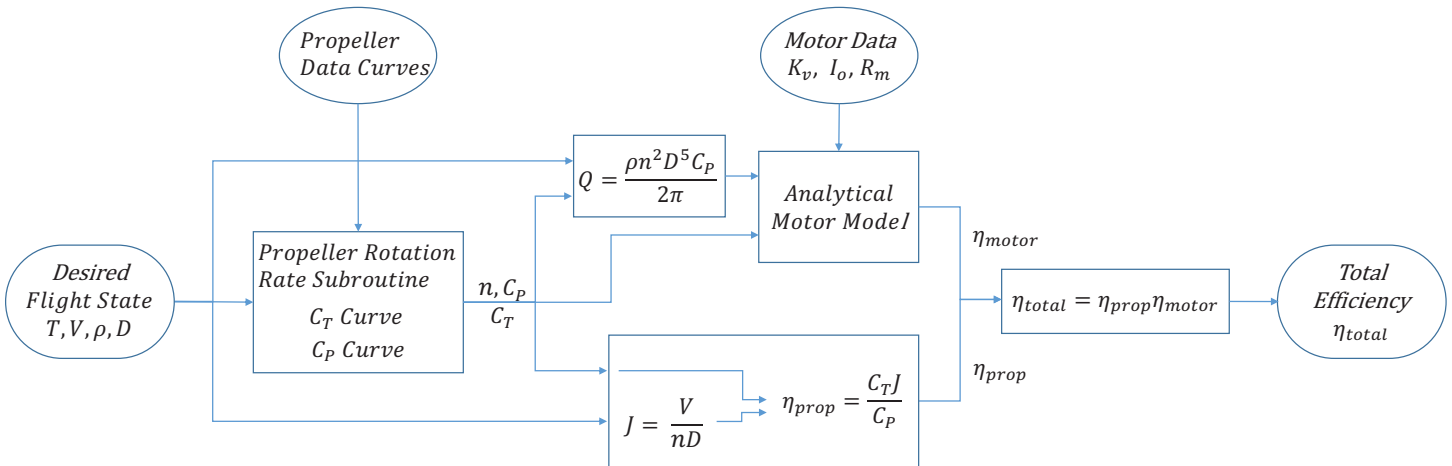
Figure 3: Process diagram of the *Flight Segment Propeller-Motor Efficiency Algorithm.*

American Institute of Aeronautics and Astronautics

```
                    ┌─────────┐
                    │  Begin  │
                    └─────────┘
                         │
          ┌──────────────────────────────┐
          │  Initialize the two closest   │
          │      C_T and n values          │
          └──────────────────────────────┘
                         │
                      ╱─────╲
                     ╱ Any C_T ╲──── false ──→ ┌─────┐
                     ╲ curves? ╱               │ End │
                      ╲─────╱                  └─────┘
                         │ true
          ┌──────────────────────────────┐  ←───┐
          │      Initialize current n     │      │
          └──────────────────────────────┘      │
                         │                        │
          ┌──────────────────────────────┐      │
          │         Calculate J            │      │
          │         J = V/nD               │      │
          └──────────────────────────────┘      │
                         │                        │
          ┌──────────────────────────────┐      │
          │      Interpolate for C_T       │      │
          └──────────────────────────────┘      │
                         │                        │
          ┌──────────────────────────────┐      │
          │    Calculate expected C_T      │      │
          │    C_T = T/(ρn²D⁴)            │      │
          └──────────────────────────────┘      │
                         │                        │
          ┌──────────────────────────────┐      │
          │   Update the two closest       │      │
          │      C_T and n values          │      │
          └──────────────────────────────┘      │
                         │                        │
                      ╱─────╲                     │
                     ╱  Any   ╲                    │
                     ╲remaining╲─── true ──────────┘
                     ╱C_T curves?╱
                      ╲─────╱
                         │ false
          ┌──────────────────────────────┐
          │  Interpolate between the two   │
          │    closest C_T polars for n    │
          └──────────────────────────────┘
                         │
          ┌──────────────────────────────┐
          │      Interpolate for C_P       │
          └──────────────────────────────┘
                         │
                    ┌─────────┐
                    │   End   │
                    └─────────┘
```
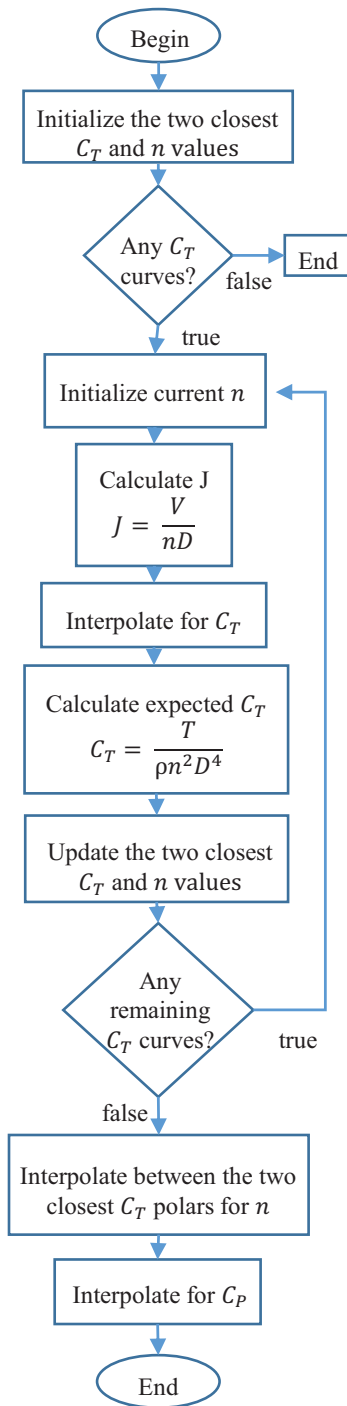
Figure 4: Process diagram of the *Propeller Rotation Rate Subroutine*.

(a)

(b)

(c)
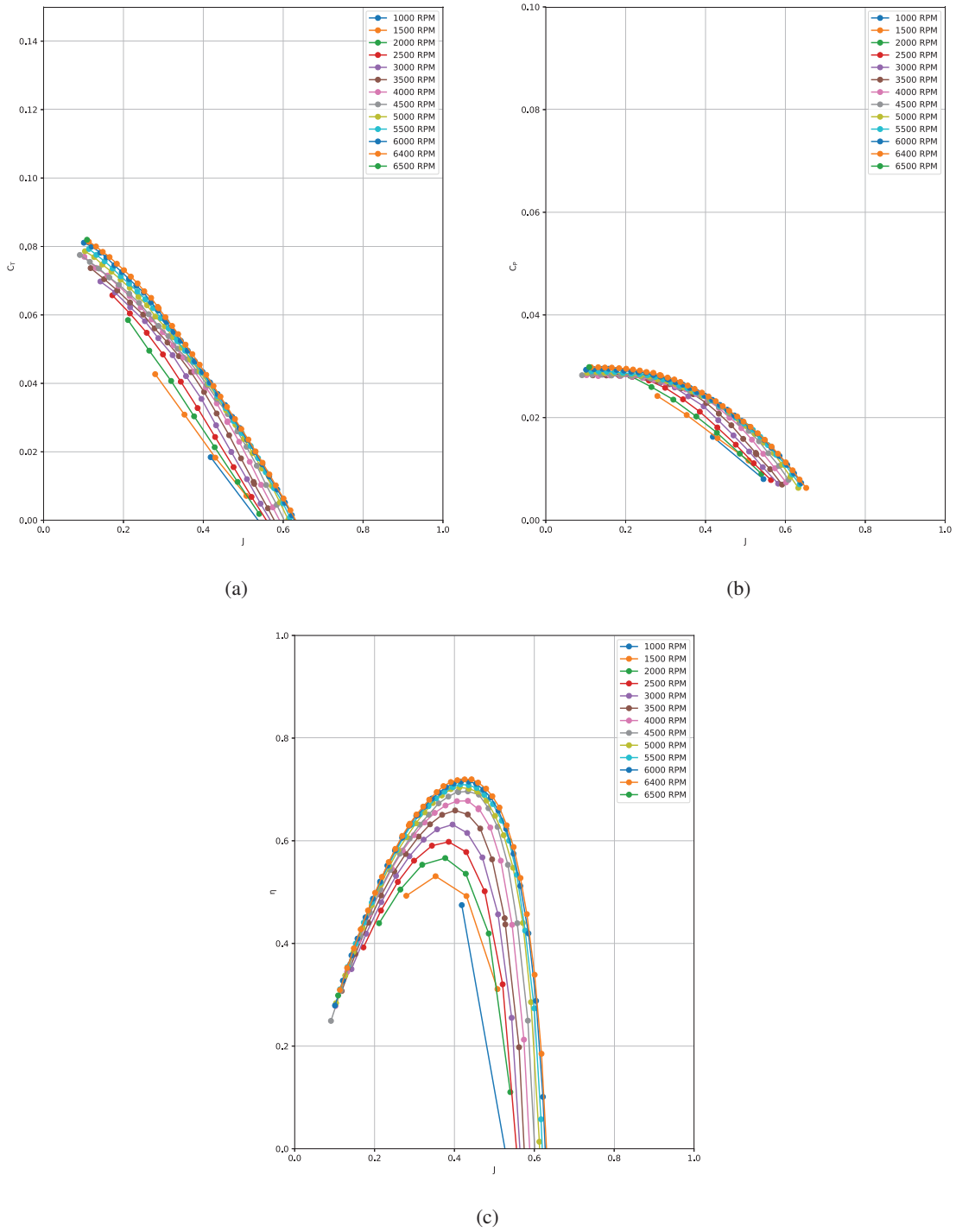
Figure 5: Example propeller performance curves: (a) thrust coefficient, (b) power coefficient, and (c) efficiency curves

B.   Maximum Thrust at Minumum Speed

In order to ensure the safe operation of the unmanned aircraft being optimized, the propulsion system optimization tool also computes the maximum thrust that each potential motor propeller combination can produce at a prescribed minimal flight speed. This functionality provides the user with quantitative thrust values which can be used to judge whether or not the propulsion system could sufficiently aid in the recovery of the aircraft from precariously low-speed situations, e.g. upset recovery scenarios following stall or spin, is sufficient.

The tool estimates the maximum thrust available for each potential propulsion system combination through a rather straightforward process. The tool starts by computing the maximum possible rotation rate for each potential motor using Equation 12, the speed constant of each potential motor, and assuming that the back emf voltage is equal to the prescribed propulsion system supply voltage (battery voltage). Then, the advance ratio is found for each of the possible combinations using Equation 3, the maximum rotation rate for each potential motor, and the diameter of each potential propeller. Finally, by interpolating between the thrust coefficient curves for all potential propeller, for each of the respective combination advance ratios, the maximum available thrust for all combinations can be found.

C.   Performance Estimation

The built-in functionality of the propulsion system optimization tool also allows for the user to compute the expected performance of a set propeller motor combination given an array of velocity and thrust values or of velocity and rotation rate values. The former of these two additional capabilities is helpful for mission planning when the exact mission profile may not be known. Thus, the user can sweep an array of possible velocity and thrust values and observe the resulting efficiency values. The latter additional capability is helpful for various post-flight analyses of propulsion system data, e.g. aerodynamic analysis requiring thrust knowledge, aircraft/propulsion system monitoring, etc. Specifically, the user is able to input an array of velocity and rotation rate values and the tool will output thrust and efficiency values. The methods by which the propulsion system optimization tool performs these additional capabilities are sub-operations of the already discussed primary and maximum thrust at minimum speed operations.

American Institute of Aeronautics and Astronautics

IV. Flight Test Validation

The propulsion system optimizer was demonstrated using an existing aircraft, the Avistar UAV, which was previously used for a variety of modeling, avionics, and flight control development.[31,36–39] The aircraft was flown using the existing motor and a baseline manufacturer recommended propeller to establish a baseline and then with an optimized propeller to demonstrate the improvement.

A. Aircraft Setup

The Avistar UAV aircraft was developed off of the Great Planes Avistar Elite fixed-wing trainer-type radio control model and has a wingspan of 1.59 m and a mass of 3.71 kg. The completed flight-ready aircraft is shown in Figure 6 and its physical specification are given in Table 1. Component specifications are given in Table 2; further details can be found in Ref. 37. The aircraft was instrumented with an Al Volo FC+DAQ flight computer and data acquisition system.[40] The specifications of the instrumentation used for flight testing are given in Table 3. The complete physical, component, and instrumentation specifications can be found in Ref. 31.

Figure 6: Flight-ready Avistar UAV.

Table 1: The Avistar UAV Aircraft Physical Specifications

Geometric Properties	
Overall Length	1395 mm (55.0 in)
Wing Span	1590 mm (62.5 in)
Wing Area	43.3 dm^2 (672 in^2)
Aspect Ratio	6.62
Inertial Properties	
Mass/Weight	
Empty (w/o Battery)	3.21 kg (7.08 lb)
4S LiPo Battery	0.50 kg (1.10 lb)
Gross Weight	3.71 kg (8.18 lb)
Wing Loading	85.6 gr/dm^2 (28.0 oz/ft^2)

American Institute of Aeronautics and Astronautics

Table 2: The Avistar UAV Airframe Component Specifications

Construction	Built-up balsa and plywood structure, aluminum wing tube, aluminum landing gear, abs canopy, and plastic film sheeted.
Flight Controls	
Controls	Aileron (2), elevator, rudder, throttle, and flaps (2)
Receiver	Futaba R6014HS
Servos	(6) Futaba S3004
Regulator	Castle Creations CC BEC
Receiver Battery	Thunder ProLiteX 2S 7.4V 500 mAh
Propulsion	
Baseline Propeller	APC 13x8E
Motor	AXI 4120/14 Outrunner
ESC	Castle Creation Phoenix ICE 75 Amp Brushless Speed Controller
Motor Flight Pack Battery	Thunder Power ProLiteX 4S 14.8 V 6.6 Ah, lithium polymer

Table 3: The Avistart UAV Instrumentation Specifications

Instrumentation system	Al Volo FC+DAQ 400 Hz system
Sensors	
Inertial	XSens MTi-G-700 AHRS with GPS
Airspeed	Al Volo pitot-static airspeed sensor
Motor Sensors	Al Volo Castle ESC sensor
Power	
Regulator	Built into FDAQ
Battery	Thunder Power ProLite 3S 1350 mAh

B.   Experiment Setup

The experimental validation testing was to be performed with the Avistar UAV flying in straight and level flight at an airspeed of 20 m/s. Due to operational constraints during the time of the validation flight testing campaign, the aircraft would be manually piloted and therefore the validation was constrained to straight and level flight as this flight condition could be performed with greatest repeatability. Based on previous flight testing experience, it was expected that the human pilot could only maintain a velocity within ± 1 m/s of the desired 20 m/s. Using a high fidelity aircraft power model that was developed in previous work,[31] the required thrust was computed to be approximately 3-5 N for the expected range of flight speeds, of 19 to 21 m/s. It should be noted that additional factors were also considered including variations in mass and center of gravity (depending on the given aircraft test configuration) and flight conditions, namely air density.

Due to practical supply limitations, the experimental validation testing was bound to the existing aircraft motor, the AXI 4120/14, and a choice of APC propeller (manufactured by Landing Products Inc.[41]); APC propellers are readily available, low cost, and have been previously performance tested.[34] The propulsion system optimization tool was then used to determine the APC propeller(s) that in combination with the AXI 4120/14 motor would provide the required thrust at the greatest operational efficiency, i.e. using the least amount of power. This propeller motor combination would be flight tested against the default combination, which was in current use.

The results of the preliminary optimization are provided in Figure 7. As can be seen in the figure, the top 6 propellers that provide the greatest efficiency are the APC 8×4 E, APC 9×9 E, APC 11×10 E, APC 9×7.5 E, APC 8×8 E, and APC 10×7 E, in that order. Beyond this point, the next propeller has similar efficiency to the default APC 13×8 E. However, it would be rather dangerous to use any of the top results, except for the APC 11×10 E, as these propellers only produce fractional amounts ($< 50\%$) of maximum thrust produced by the APC 13×8 E at the stall speed of the aircraft, i.e. these propellers would not allow a margin of safety in flight testing. Therefore the APC 11×10 E, was the sole propeller chosen for a flight testing comparison with the APC 13×8 E. These propellers are shown in Fig. 8.

American Institute of Aeronautics and Astronautics
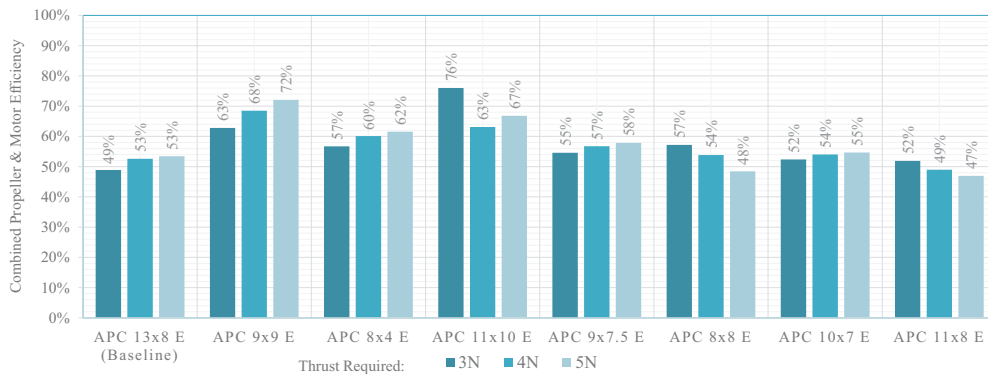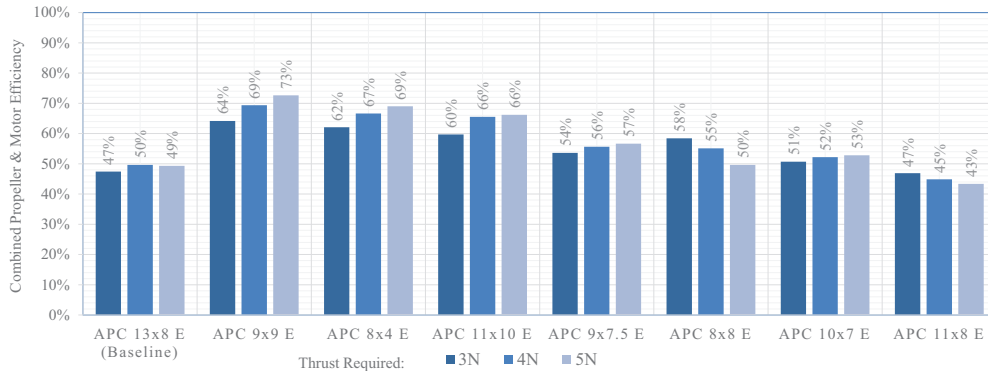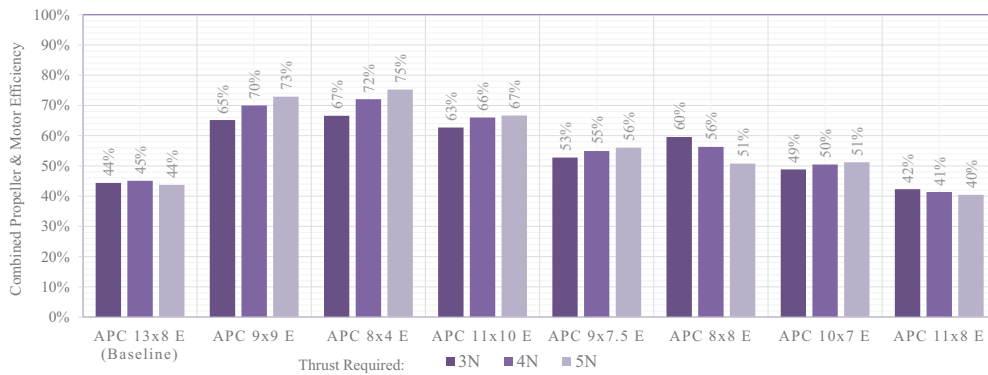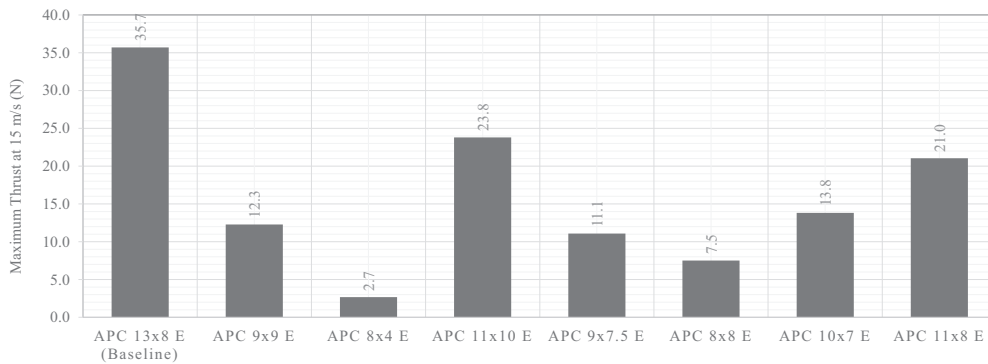
Figure 7: Comparison of motor propeller efficiency for required thrusts of 3, 4, and 5*N* at: (a) 19 m/s, (b) 20 m/s, and (c) 21 m/s and (d) the maximum thrust available at 15 m/s for AXI 4120/14 motor with various APC E propellers.

American Institute of Aeronautics and Astronautics

Figure 8: A photo of the two propellers tested: APC 11×10 E (top) and APC 13×8 E (bottom)

C. Results

The Avistar UAV was piloted in straight and level flight at approximately 20 m/s with the AXI 4120/14 motor and the APC 13×8 E and APC 11×10 E, respectively. In order to minimize environmental effects, specifically thermals and horizontal wind that could effect the thrust required by the aircraft, flight testing was constrained to pre-dusk periods with stable temperatures and lows winds; these constraints limited flight testing to 3 days during the early-summer of 2019.

Data produced from the flight testing was filtered for flight segments of at least 5 seconds with zero control input, minimal pitch and roll ($<$ 5 deg), minimal climb rate ($<$ 0.5 m/s), and near-constant propeller rotation rate ($< \pm$100 RPM). In total, 5 data points were measured for each of the two propeller, each averaged from thousands of individual airspeed, propeller rotation rate, voltage, current samples logged at 400 Hz. The average voltage and current measurements (measured at the ESC providing motor power consumption) were used to compute the *measured power* while the averaged airspeed and propeller rotation rate measurements were used to compute the *computed thrust* and *computed power*.

In order to confirm that the aircraft aerodynamics and thrust required has not changed by changing the propeller, the computed thrust was plotted against the measured airspeed for the two tested combinations in Fig. 9. There is good agreement between the two combinations, indicating that the aircraft requires (nearly) identical thrust at the same flight condition. Interestingly, there is a trend where thrust required decreases as the airspeed increases. This is explained by the fact that the aircraft is operating slower than its peak efficiency (where L/D is maximized).[42]

Finally, Fig. 10 show the computed thrust plotted against the measured airspeed for the two tested motor propeller combinations without and with error bars. In Fig. 10(a), the measured and computed results show that the optimized AXI 4120/14 motor and APC 11×10 E propeller combination requires approximately 20% less power than the default AXI 4120/14 motor and APC 13×8 E propeller combination. There are similar trends for the measured and computed power requirements within each combination however, there are decently large deviations especially at lower speeds. The majority of deviations can be explained by instrument measurement uncertainty. Specifically, the instrumentation used in-flight is only able to measure propeller rotation rate and airspeed within an accuracy of $\pm$ 100 RPM and $\pm$ 0.5 m/s, respectively. These ranges can be taken into account and an acceptable error range can be co-plotted with error bars. In Fig. 10(b), the same measured and computed results are co-plotted with the addition of error bars for the instrument accuracy. The measured results are plotted with error bars for velocity offsets of $\pm$ 20 m/s (as rotation rate measurement error do not effect their values) while the computed results are plotted with error bar boundaries for the $\pm$ 100 RPM rotation rate and $\pm$ 0.5 m/s velocity offsets. 9 out of the 10 measured data error bars overlap with computed data error bar boundaries signifying that there is good agreement between the measured and computed power data when considering measurement uncertainty.

American Institute of Aeronautics and Astronautics
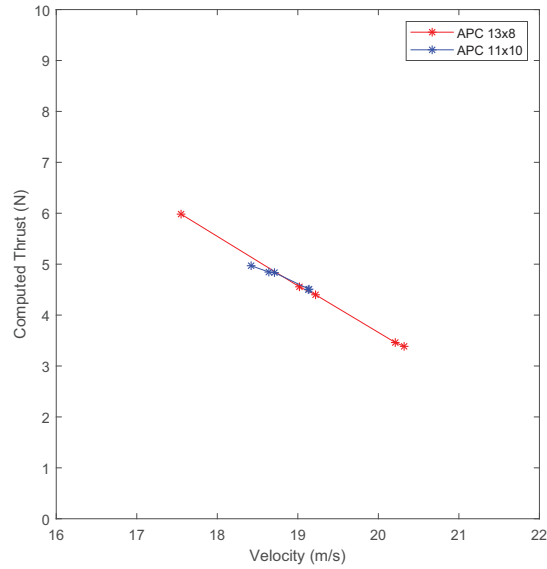
Figure 9: Computed thrust vs. measured airspeed for the AXI 4120/14 motor and the APC 13×8 E and APC 11×10 E, respectively, in straight and level flight with the Avistar UAV.

(a)

(b)
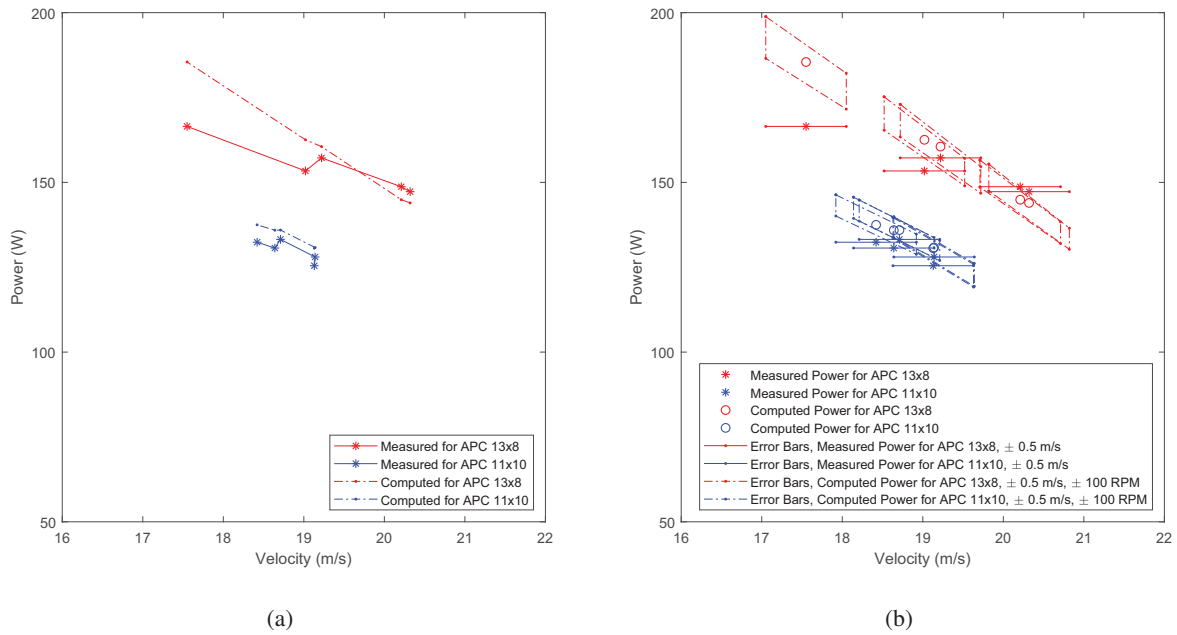
Figure 10: Measured and computed power consumption vs. measured airspeed for the AXI 4120/14 motor and the APC 13×8 E and APC 11×10 E, respectively, in straight and level flight with the Avistar UAV, (a) without and (b) with error bars.

American Institute of Aeronautics and Astronautics

V.   Mission Simulation

The propulsion optimization tool was applied to the simulations of two potential missions that the Avistar UAV could perform [a]. These missions include a field coverage flight and a long-distance, multiple-site inspection flight. For each mission, the propulsion optimization tool analyzed over 1300 potential combinations. Below, the profiles of these missions are presented and along with the results from the propulsion system optimization tool. Note that for simplicity of the simulations, the turn and climb transitions as well as velocity changes were assumed to occur instantaneously; previous work[43] has modeled these transitions and could be integrated into future propulsion system optimization work.

A.   Field Coverage Mission

The first simulated mission presented is a 1 km by 1 km field coverage flight. A trajectory plot of the mission is presented in Fig. 11. The mission begins with a takeoff followed by a 15 degree climb to 50 m in altitude. The aircraft then turns toward the desired area and flies approximately 400 m. It then maneuvers an proceeds to fly a zig-zag field coverage with 50 m radius turn arounds after each pass. The field is covered with 11 passes after which point the aircraft flies back toward the runway, maneuvers, and finally descends. The entire mission is flown at 20 m/s with exception of the climb out after takeoff and descent to landing. The resulting simulated state data for position, Euler angles, and velocity are presented in Fig. 12. The figure also contains thrust requirement predictions generated by the aforementioned aircraft power model.[31] The velocity and thrust profiles were fed into the optimizer along with a list of potential motors and propellers that could feasibly used on the aircraft.

The propulsion system optimization tool produced a table of potential combinations along with estimated input energy consumption, overall-average efficiency, and maximum thrust at the minimum speed of 15 m/s. Table 4 presents the 25 most efficient propeller motor combinations as well as the baseline combination, which was ranked at 410, and their respective performance estimates for the field coverage mission. As can be seen from the table, there is a significant, ∼50% relative improvement in efficiency, from 49.6% for the baseline propeller and motor combination to ≥74% for the top 7 propeller motor combinations. However, as is expected, there is a reduction in maximum thrust at the minimum speed of 15 m/s for the most efficient propellers motor combinations, compared to the baseline combination. Due to this decrease, one would choose the 3rd or 4th ranked combination as it likely offers sufficient safe maximum thrust at the minimum speed of 15 m/s.
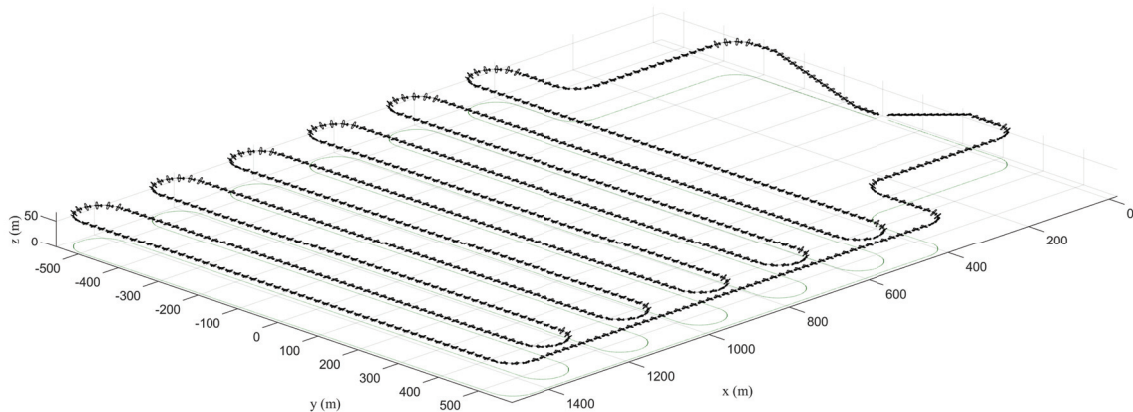
Figure 11: Trajectory plot of the simulated 1 km by 1 km field coverage flight mission (the aircraft is plotted 8x scale every 1.0 s).

---

[a]The aircraft could perform the simulated missions in real life with proper certification and licensing from a governing aviation body, e.g. FAA.

American Institute of Aeronautics and Astronautics
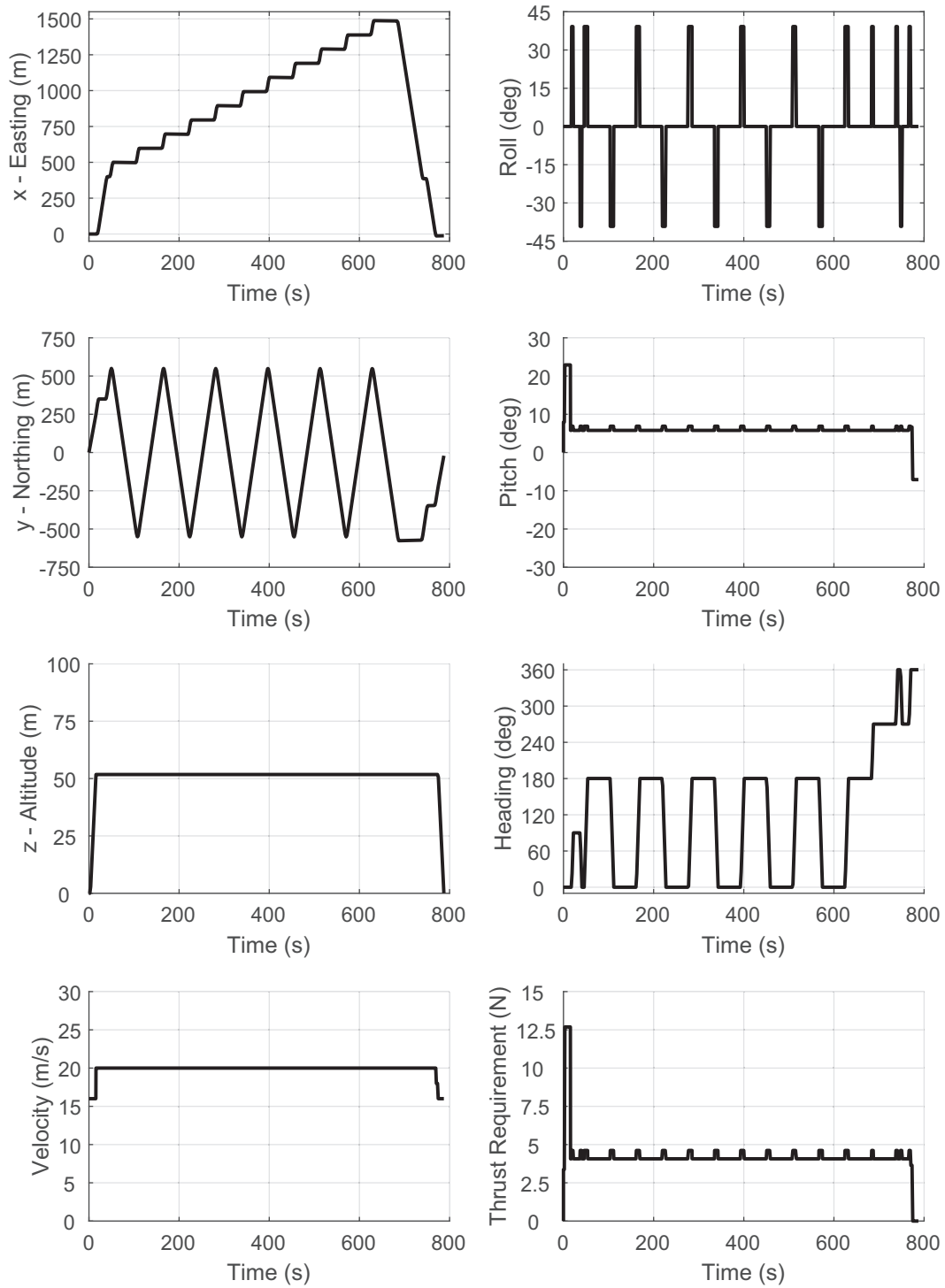
Figure 12: A time history of the simulated 1 km by 1 km field coverage flight mission.

American Institute of Aeronautics and Astronautics

Table 4: The Propulsion System Optimization Results for the Simulated 1 km by 1 km Field Coverage Flight Mission

Ranking	Propeller	Motor	Total Energy (J)	Average Efficiency (%)	Maximum Thrust (N)
1	APC 9×9 E	Hacker A40-10S V4	87,614	74.7	16.3
2	APC 9×9 E	Hacker A40-14L V4	87,657	74.7	2.6
3	APC 9×9 E	Neu 1512/5.5D	88,113	74.3	23.8
4	APC 9×9 E	Neu 1512/5D	88,303	74.1	28.8
5	APC 9×9 E	Hacker A40-10L V4	88,400	74.0	6.5
6	APC 9×9 E	Hacker A40-12L V4	88,408	74.0	4.0
7	APC 9×9 E	Neu 1512/5.75D	88,436	74.0	21.8
8	APC 9×9 E	Neu 1512/5.25D	88,540	73.9	26.0
9	APC 9×9 E	Neu 1512/6D	88,709	73.8	19.9
10	APC 9×9 E	Hacker A40-14S V4	89,023	73.5	7.4
11	APC 9×9 E	Hacker A40-8L V4	89,071	73.5	10.3
12	APC 9×9 E	Hacker A40-12S V4	90,310	72.5	10.3
13	APC 9×9 E	Hacker A50-14S V4	90,588	72.2	4.4
14	APC 9×9 E	Hacker A50-14XS V4	90,666	72.2	7.1
15	APC 9×9 E	Hacker A50-16S V4	91,367	71.6	2.8
16	APC 9×9 E	Hacker A50-16L V4	91,601	71.4	0.4
17	APC 9×9 E	AXi 4120/18	91,712	71.4	6.9
18	APC 9×9 E	Hacker A50-12S V4	92,135	71.0	5.9
19	APC 9×9 E	Great Planes Rimfire 42-60-480	92,272	70.9	5.9
20	APC 11×10 E	Hacker A40-14L V4	92,336	70.9	5.6
21	APC 11×10 E	Hacker A40-12L V4	93,052	70.3	8.2
22	APC 11×10 E	Hacker A40-10L V4	93,153	70.2	13.0
23	APC 9×9 E	AXi 4120/14	93,330	70.1	12.3
24	APC 11×10 E	Hacker A40-8L V4	93,697	69.8	20.1
25	APC 9×9 E	Hacker A50-12L V4	93,756	69.8	2.6
410	APC 13×8 E	AXi 4120/14	132,047	49.6	35.7

B. Long-Distance, Multiple-Site Inspection Mission

The second simulated mission presented is a 6-site inspection flight about an 8 km^2 area. A trajectory plot of the mission is presented in Fig. 13. The mission begins with a takeoff followed by a 15 deg climb to 100 m in altitude. The aircraft then turns toward the first inspection point and flies approximately 1500 m. After circling the first inspection point with a 100 m radius, it orients towards the next closest point 1000 m away. This is repeated a total of 6 times in a hexagonal fashion; note that the inspection points were laid out in this pattern for ease of simulation, however, the pattern can be arbitrary. After the last inspection is made, the aircraft flies back toward the runway, maneuvers, and finally descends. The entire second mission is flown slightly faster than the first at 23 m/s, again with exception of the climb out after takeoff and descent to landing. The resulting simulated state data for position, Euler angles, and velocity are presented in Fig. 14. The figure also contains thrust requirement predictions, again generated by the aforementioned aircraft power model. These velocity and thrust profiles were fed into the optimizer again with a list of potential motors and propellers that could feasibly used on the aircraft.

For the second mission, the propulsion system optimization tool produced a second table of potential combinations and performance estimates. Table 5 presents the 25 most efficient combinations as well as the baseline combination, which was ranked at 360, for the second mission. As can be seen from the table, there is an even more significant relative improvement in efficiency compared to the first mission, of 80% relative, from 38.6% for the baseline combination to $\geq$70% for the top 13 combinations. Again, as is expected, there is a reduction in maximum thrust at the minimum speed these combinations, compared to the baseline combination. Here, due to the large decrease, one would likely choose the 15th ranked combination as it offers an almost equal safe maximum thrust at the minimum speed. It is interesting to note that the 18th, 20th — 23rd, and 25th combinations actually offers more thrust available at minimum speed than the baseline combination, albeit at relative efficiency improvements of only 73—75%.
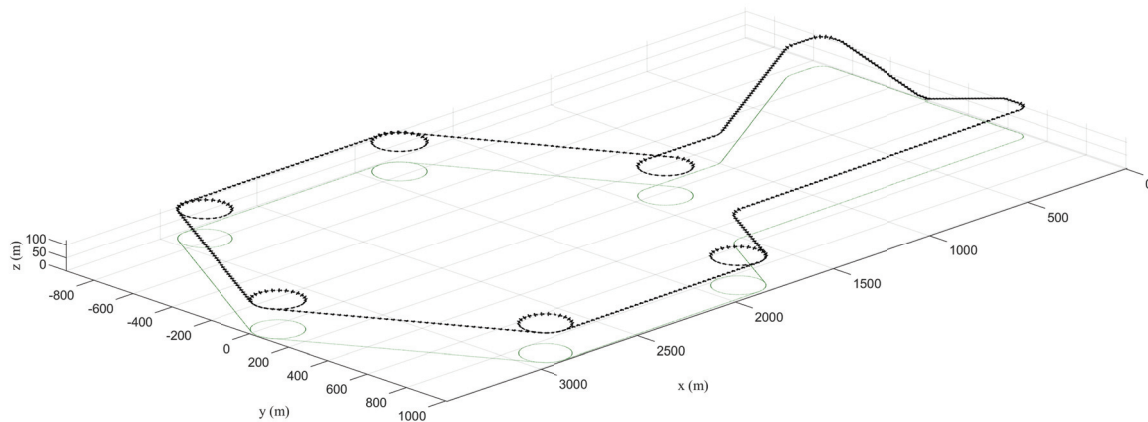
Figure 13: Trajectory plot of the simulated long-distance, multiple-site inspection flight mission (the aircraft is plotted 8x scale every 1.0 s).

American Institute of Aeronautics and Astronautics
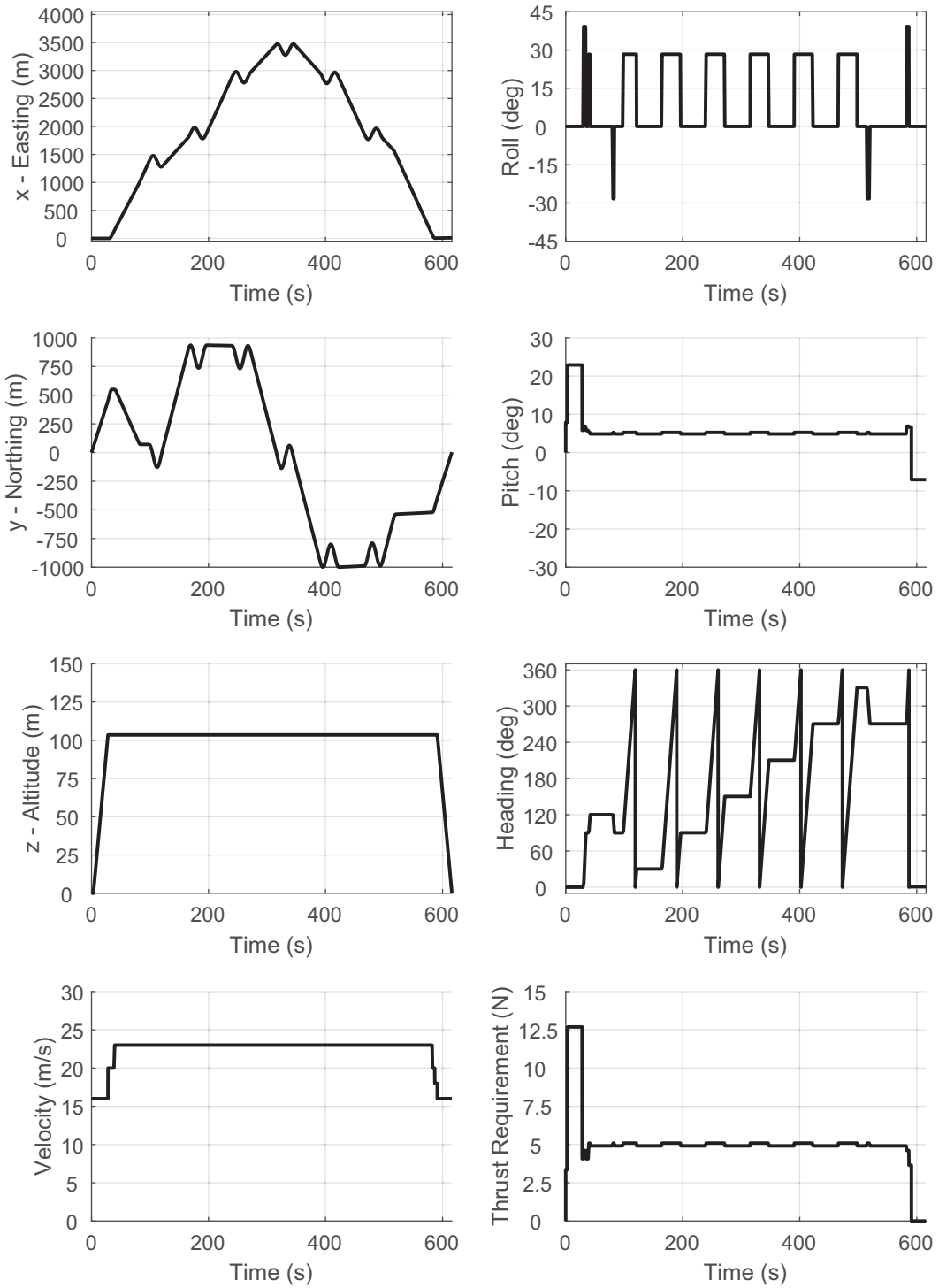
Figure 14: A time history of the simulated long-distance, multiple-site inspection flight mission.

Table 5: The Propulsion System Optimization Results for the Simulated Long-Distance, Multiple-Site Inspection Flight Mission

Ranking	Propeller	Motor	Total Energy (J)	Average Efficiency (%)	Maximum Thrust (N)
1	APC 11×10 E	Hacker A40-14L V4	94,241	73.1	5.6
2	APC 11×10 E	Hacker A40-12L V4	94,878	72.6	8.2
3	APC 11×10 E	Hacker A40-10L V4	95,094	72.4	13.0
4	APC 11×10 E	Hacker A40-8L V4	95,465	72.1	20.1
5	APC 11×10 E	Hacker A40-14S V4	95,825	71.9	14.8
6	APC 11×10 E	Hacker A50-14S V4	95,925	71.8	8.9
7	APC 11×10 E	Hacker A50-14XS V4	96,268	71.5	14.2
8	APC 11×10 E	Hacker A50-16L V4	96,303	71.5	1.5
9	APC 11×10 E	Hacker A50-16S V4	96,425	71.4	6.1
10	APC 11×10 E	Hacker A40-12S V4	96,595	71.3	20.1
11	APC 11×10 E	Hacker A50-12S V4	97,032	71.0	11.9
12	APC 11×10 E	Hacker A50-12L V4	98,002	70.3	5.6
13	APC 11×10 E	Hacker A50-14L V4	98,416	70.0	3.1
14	APC 11×10 E	Rimfire 42-60-480	98,696	69.8	11.9
15	APC 11×10 E	Hacker A40-10S V4	99,059	69.5	31.3
16	APC 11×10 E	AXi 4120/18	100,248	68.7	13.9
17	APC 11×10 E	AXi 4120/14	100,368	67.9	23.8
18	APC 11×10 E	Neu 1512/5.5D	101,697	67.7	46.0
19	APC 11×10 E	AXi 4120/20	101,843	67.6	11.1
20	APC 11×10 E	Neu 1512/5D	101,921	67.6	56.2
21	APC 11×10 E	Neu 1512/5.75D	102,049	67.5	41.9
22	APC 11×10 E	Neu 1512/5.25D	102,103	67.5	50.7
23	APC 11×10 E	Neu 1512/6D	102,314	67.3	38.3
24	APC 11×10 E	Rimfire 42-60-600	102,850	67.0	19.4
25	APC 11×10 E	Neu 1708/1.5Y	103,059	66.8	40.8
360	APC 13×8 E	AXi 4120/14	178,654	38.6	35.7

American Institute of Aeronautics and Astronautics

C.   Discussion of Simulated Mission Results

It is interesting to note a few observation about the results of both missions. First, it is interesting that the 24th ranked combination in the first mission, the APC 11×10E propeller and Hacker A40-8L V4, is the 4th ranked combination in the second mission. This observation signifies that the combination may be good for a variety of missions. However, it should be mentioned that this combination only produces 20 N of thrust at the minimum speed, which may or may not be enough to safely propel the aircraft.

A second observation is that the Neu 1512/5.5D motor, which ranks 3rd in the first mission with the APC 9×9E propeller, ranks 18th in the second mission with the APC 11×10E propeller. In the first mission, the combination produces debatably enough maximum thrust at the minimum speed and actually exceeds the maximum thrust at the minimum speed of the baseline combination in the second mission. Therefore, a potential user could install the Neu 1512/5.5D motor on the aircraft and solely switch propellers between flights to both significantly increase the propulsion system efficiency as well as provide sufficient thrust to recover from precarious slow-speed scenarios. It should be mentioned that the Neu 1512/5D motor also has similar behavior between the two missions and could be used in a similar manner if the Neu 1512/5.5D motor was unavailable.

VI.   Summary and Future Work

This paper described a propulsion system optimization tool that determines the optimal propeller and motor combination(s) for an electric, fixed-wing unmanned aircraft, given desired mission requirements. Specifically, potential missions are broken down into expected segments with velocity and thrust requirements that are based on the mission profile and were computed using a high-fidelity aircraft power model. The optimization tool then estimates the required propeller rotation rate, followed by the power consumption for each segment and propeller-motor combination. It then integrates the segment results for each combination and tabulates the results, sorting by overall efficiency.

Among a variety of additional functionality integrated into the tool, the optimizer considers aircraft safety by estimating the maximum thrust that each combination can produce, which is crucial in upset recovery scenarios such as stall. Additionally, the tool is able to compute a combination's performance for a set or sweep of velocities and thrusts, either as required by a flight condition or from flight test data; this is helpful for mission planning and post-flight analysis. The optimization tool and its additional functionalities were experimentally validated through flight testing of a previously developed and well-characterized unmanned aircraft. Additionally, propulsion system optimization of two simulated missions was performed, demonstrating the energy saving that can be made.

Experimental validation testing of the optimization tool was performed through flight testing of a previously developed and well-characterized unmanned aircraft. The propulsion system optimization tool was then applied to two distinct simulated missions that the tested aircraft could perform. These missions include a field coverage flight and a long-distance, multiple-site inspection flight. For each mission, the propulsion optimization tool analyzed over 1300 potential combinations. The results showed that optimized combinations of propellers and motors were able to achieve relative efficiency improvements of 50 to 80% compared to the baseline combination. Additionally, propeller motor combinations were found that offered significant improvements for both propeller while maintaining high maximum thrust at minimum speeds. This results is especially paramount for long-endurance, solar-powered aircraft.

For future work, additional flight testing is planned with the use of a flight testing automation autopilot module.[39] The flight testing automation module will enable more precise trajectories to be flown than were possible through manual human piloting. Additional validation testing is planned where the aircraft would fly a more repeatable and evenly distributed sweep of conditions, i.e. velocities. Additionally, flight testing of potential example missions is also desired in order to demonstrate real world efficiency gains that can be made though using the propulsion system optimization tool.

Acknowledgments

References

[1]Altavian, "Products - Altavian," http://www.altavian.com/Products, Accessed Apr. 2015.

[2]Precision Hawk, "Precision Agriculture, Commercial UAV and Farm Drones For Sale," http://precisionhawk.com/, Accessed Apr. 2015.

[3]MicroPilot, "MicroPilot - MP-Vision," http://www.micropilot.com/products-mp-visione.htm, Accessed Apr. 2015.

[4]Dantsker, O. D., Theile, M., and Caccamo, M., "Design, Development, and Initial Testing of a Computationally-Intensive, Long-Endurance Solar-Powered Unmanned Aircraft," AIAA Paper 2018-4217, AIAA Applied Aerodynamics Conference, Atlanta, Georgia, June 2018.

[5]Real Time and Embedded System Laboratory, University of Illinois at Urbana-Champaign, "Solar-Powered Long-Endurance UAV for Real-Time Onboard Data Processing," http://rtsl-edge.cs.illinois.edu/UAV/, Accessed Jan. 2018.

[6]Green, C. R. and McDonald, R. A., "Modeling and Test of the Eciency of Electronic Speed Controllers for Brushless DC Motors," AIAA Paper 2015-3191, AIAA Aviation Forum, Dallas, Texas, Jun. 2015.

[7]McCrink, M. H. and Gregory, J. W., "Blade Element Momentum Modeling for Low-Re Small UAS Electric Propulsion Systems," AIAA Paper 2015-3191, AIAA Aviation Forum, Dallas, Texas, Jun. 2015.

[8]Lundstrom, D., Amadori, K., and Krus, P., "Validation of Models for Small Scale Electric Propulsion Systems," AIAA Paper 2010-483, AIAA Aerospace Sciences Meeting, Orlando, Florida, Jan. 2010.

[9]Brandt, J. B., *Small-Scale Propeller Performance at Low Speeds*, Master's thesis, University of Illinois at Urbana-Champaign, Department of Aerospace Engineering, Urbana, IL, 2005.

[10]Bradt, J. B. and Selig, M. S., "Propeller Performance Data at Low Reynolds Numbers," *AIAA Aerospace Sciences Meeting, Orlando, Florida, Jan. 2011*.

[11]Lundstrom, D. and Krus, P., "Testing of Atmospheric Turbulence Effects on the Performance of Micro Air Vehicles," *International Journal of Micro Air Vehicles*, Vol. 4, No. 2, Jun. 2012, pp. 133–149.

[12]Lindahl, P., Moog, E., and Shaw, S. R., "Simulation, Design, and Validation of an UAV SOFC Propulsion System," *IEEE Transactions on Aerospace and Electronic Systems*, Vol. 48, No. 3, JULY 2012, pp. 2582–2593.

[13]Uhlig, D. V., *Post Stall Propeller Behavior at Low Reynolds Numbers*, Master's thesis, University of Illinois at Urbana-Champaign, Department of Aerospace Engineering, Urbana, IL, 2007.

[14]Uhlig, D. V. and Selig, M. S., "Post Stall Propeller Behavior at Low Reynolds Numbers," *AIAA Paper 2008-407, AIAA Aerospace Sciences Meeting, Reno, Nevada, Jan. 2008*.

[15]Deters, R. W. and Selig, M. S., "Static Testing of Micro Propellers," AIAA Paper 2008-6246, AIAA Applied Aerodynamics Conference, Honolulu, Hawaii, Aug. 2008.

[16]Chaney, C. S., Bahrami, J. K., Gavin, P. A., Shoemake, E. D., Barrow, E. S., and Matveev, K. I., "Car-Top Test Module as a Low-Cost Alternative to Wind Tunnel Testing of UAV Propulsion Systems," *Journal of Aerospace Engineering*, Vol. 27, No. 6, Nov. 2014.

[17]Deters, R. W., *Performance and Slipstream Characteristics of Small-Scale Propelllers at Low Reynolds Numbers*, Ph.D. thesis, University of Illinois at Urbana-Champaign, Department of Aerospace Engineering, Urbana, IL, 2014.

[18]Deters, R. W., Kleinke, S., and Selig, M. S., "Static Testing of Propulsion Elements for Small Multirotor Unmanned Aerial Vehicles," AIAA Paper 2017-3743, AIAA Aviation Forum, Denver, Colorado, June 2017.

[19]Dantsker, O. D., Selig, M. S., and Mancuso, R., " A Rolling Rig for Propeller Performance Testing," AIAA Paper 2017-3745, AIAA Applied Aerodynamics Conference, Denver, Colorado, June 2017.

[20]Gong, A. and Verstraete, D., "Experimental Testing of Electronic Speed Controllers for UAVs," AIAA Paper 2017-4955, AIAA/SAE/ASEE Joint Propulsion Conference, Atlanta, Georgia, July 2017.

[21]Gong, A., Maunder, H., and Verstraete, D., "Development of an in-fight thrust measurement system for UAVs," AIAA Paper 2017-5092, AIAA/SAE/ASEE Joint Propulsion Conference, Atlanta, Georgia, July 2017.

[22]Gong, A., MacNeill, R., and Verstraete, D., "Performance Testing and Modeling of a Brushless DC Motor, Electronic Speed Controller and Propeller for a Small UAV," AIAA Paper 2018-4584, AIAA Propulsion and Energy Forum, Cincinnati, Ohio, July 2018.

[23]Deters, R. W., Dantsker, O. D., Kleinke, S., Norman, N., and Selig, M. S., "Static Performance Results of Propellers Used on Nano, Micro, and Mini Quadrotors," AIAA Paper 2018-4122, AIAA Aviation Forum, Atlanta, Georgia, June 2018.

American Institute of Aeronautics and Astronautics

[24]Drela, M., "DC Motor / Propeller Matching," http://web.mit.edu/drela/Public/web/qprop/ motorprop.pdf.

[25]Mark Drela, "QPROP," http://web.mit.edu/drela/Public/web/qprop/, Accessed Jan. 2019.

[26]Lundstrom, D., *Aircraft Design Automation and Subscale Testing*, Ph.D. thesis, Linkoping University, Department of Management and Engineering, Linkoping, Sweden, 2012.

[27]MacNeill, R., Verstraete, D., and Gong, A., "Optimisation of Propellers for UAV Powertrains," AIAA Paper 2017-5090, AIAA/SAE/ASEE Joint Propulsion Conference, Atlanta, Georgia, July 2017.

[28]Macneill, R. and Verstraete, D., "Optimal Propellers for a Small Hybrid Electric Fuel-Cell UAS," AIAA Paper 2018-4981, AIAA/IEEE Electric Aircraft Technologies Symposium, Cincinnati, OH, July 2018.

[29]Drela, M., "First-Order DC Electric Motor Model," http://web.mit.edu/drela/Public/web/qprop/motor1_theory.pdf.

[30]Drela, M., "Second-Order DC Electric Motor Model," http://web.mit.edu/drela/Public/web/qprop/motor2_theory.pdf.

[31]Dantsker, O. D., Theile, M., and Caccamo, M., "A High-Fidelity, Low-Order Propulsion Power Model for Fixed-Wing Electric Unmanned Aircraft," AIAA Paper 2018-5009, AIAA/IEEE Electric Aircraft Technologies Symposium, Cincinnati, OH, July 2018.

[32]Landing Products Inc., "APC Propeller Performance Data," https://www.apcprop.com/technical-information/performance-data/, Accessed Feb. 2018.

[33]Martin Hepperle, "Java Prop," https://www.mh-aerotools.de/airfoils/javaprop.htm, Accessed Jun. 2019.

[34]UIUC Applied Aerodynamics Group, "UIUC Propeller Data Site," http://m-selig.ae.illinois.edu/props/propDB.html.

[35]O. Dantsker and R. Mancuso and M. Vahora, "Unmanned Aerial Vehicle Database," http://uavdb.org/.

[36]Mancuso, R., Dantsker, O. D., Caccamo, M., and Selig, M. S., "A Low-Power Architecture for High Frequency Sensor Acquisition in Many-DOF UAVs," Submitted to International Conference on Cyber-Physical Systems, Berlin, Germany, April 2014.

[37]Dantsker, O. D., Mancuso, R., Selig, M. S., and Caccamo, M., "High-Frequency Sensor Data Acquisition System (SDAC) for Flight Control and Aerodynamic Data Collection Research on Small to Mid-Sized UAVs," AIAA Paper 2014-2565, AIAA Applied Aerodynamics Conference, Atlanta, Georgia, June 2014.

[38]Dantsker, O. D., Loius, A. V., Mancuso, R., Caccamo, M., and Selig, M. S., "SDAC-UAS: A Sensor Data Acquisition Unmanned Aerial System for Flight Control and Aerodynamic Data Collection," *AIAA Infotech@Aerospace Conference, Kissimee, Florida, Jan 2015.*.

[39]Dantsker, O. D., Yu, S., Vahora, M., and Caccamo, M., "Flight Testing Automation to Parameterize Unmanned Aircraft Dynamics," AIAA Paper 2019-3230, AIAA Aviation and Aeronautics Forum and Exposition, Dallas, Texas, June 2019.

[40]Al Volo LLC, "Al Volo: Flight Systems," http://www.alvolo.us, Accessed Jun. 2019.

[41]Landing Products Inc., "APC Propellers," https://www.apcprop.com/, Accessed Feb. 2018.

[42]Yechout, T. R., Morris, S. L., Bossert, D. E., Hallgren, W. F., and Hall, J. K., *Introduction to Aircraft Flight Mechanics, 2nd Edition*, American Institute of Aeronautics and Astronautics, Inc., Reston, VA, 2014.

[43]Theile, M., Yu, S., Dantsker, O. D., and Caccamo, M., "Trajectory Estimation for Geo-Fencing Applications on Small-Size Fixed-Wing UAVs," IEEE International Conference on Intelligent Robots and Systems, Macau, China, Nov. 2019.